Journal of Systems Engineering and Electronics
Vol. 31, No. 6, December 2020, pp.1206 – 1215

Parameter estimation of GTD model and RCS extrapolation based on a modified 3D-ESPRIT algorithm

ZHENG Shuyu[1,*], ZHANG Xiaokuan[1], ZHAO Weichen[2], ZHOU Jianxiong[3], ZONG Binfeng[1], and XU Jiahua[1]

1. Air and Missile Defense College, Air Force Engineering University, Xi'an 710051, China;
2. College of Economics, Jilin University of Finance and Economics, Changchun 130022, China;
3. School of Electronics Science and Engineering, National University of Defense Technology, Changsha 410073, China

Abstract: The noise robustness and parameter estimation performance of the classical three-dimensional estimating signal parameter via rotational invariance techniques (3D-ESPRIT) algorithm are poor when the parameters of the geometric theory of the diffraction (GTD) model are estimated at low signal-to-noise ratio (SNR). To solve this problem, a modified 3D-ESPRIT algorithm is proposed. The modified algorithm improves the parameter estimation accuracy by proposing a novel spatial smoothing technique. Firstly, we make cross-correlation of the auto-correlation matrices; then by averaging the cross-correlation matrices of the forward and backward spatial smoothing, we can obtain a novel equivalent spatial smoothing matrix. The formula of the modified algorithm is derived and the performance of this improved method is also analyzed. Then we compare root-mean-square-errors (RMSEs) of different parameters and the locating accuracy obtained by different algorithms. Furthermore, radar cross section (RCS) of radar targets is extrapolated. Simulation results verify the effectiveness and superiority of the modified 3D-ESPRIT algorithm.

Keywords: parameter estimation, novel spatial smoothing, scattering center, geometric theory of diffraction (GTD) model, radar cross section (RCS) extrapolation.

DOI: 10.23919/JSEE.2020.000065

1. Introduction

The geometrical theory of diffraction (GTD) model [1] is a classical scattering center model to describe the electromagnetic characteristics of radar targets at high frequencies. In the past decades, the GTD model has wide applications in many military fields, such as targets recognition [2−7], radar cross section (RCS) extrapolation [8−10], and three-dimensional (3D) reconstruction [11−14]. Hence, building a high-precise GTD model is vitally important for radar targets electromagnetic characteristics analysis. Obviously, accurate estimated parameters have become the key to constructing a high-precision GTD model. Therefore, researchers have applied many algorithms to extract the GTD model parameters from back-scattering data of radar targets, such as the estimating signal parameter via rotational invariance techniques (ESPRIT) algorithm [15−18], the multiple signal classification (MUSIC) algorithm [19−22], the matrix enhancement and matrix pencil (MEMP) algorithm [23−25] and so on. While the parameter estimation performance of the ESPRIT algorithm is poor at low signal-to-noise ratio (SNR). Though the MUSIC algorithm performs better than the ESPRIT algorithm at low SNR conditions, it needs spectral peak searching, which burdens a heavy computation. The MEMP algorithm mismatches the closed parameters and hence it needs a parameter matching process.

In this paper, to estimate the GTD model parameters in a higher accuracy at low SNR as well as to avoid mismatched parameters, a modified 3D-ESPRIT algorithm is presented. Firstly, we add a novel correlation matrix into the traditional forward-backward spatial smoothing and obtain a new total covaraince matrix. Then by squaring the total covariance matrix, we can get the final covariance matrix. Finally, based on the final covariance and spatial spectrum estimation algorithm, we can extract the GTD model parameters. The proposed algorithm fully uses the back-scattering data of radar targets as well as broadens the differences between eigenvalues of signals and eigenvalues of noises simultaneously. Simulation results verify the effectiveness and superiority of our proposed algorithm.

This paper is organized as follows: Section 2 introduces the 3D-GTD model. Section 3 presents the pro-

Manuscript received December 23, 2019.
*Corresponding author.
This work was supported by the National Natural Science Foundation of China (61372033).

posed modified 3D-ESPRIT algorithm to estimate the GTD model parameters. Section 4 provides the simulations and the computational analysis. Finally, Section 5 concludes this paper.

2. The 3D-GTD scattering center model

As a classical scattering center model, the GTD model can describe the electromagnetic characteristics of radar targets. At high frequencies, the GTD model of targets [12] can be expressed as

$$E(f_m,\theta_n,\varphi_k)=\sum_{i=1}^{I}A_i\left(\mathrm{j}\frac{f_m}{f}\right)^{\alpha_i}\exp[-4\pi\mathrm{j}f_m(x_i\cos\theta\cos\varphi+ y_i\sin\theta\cos\varphi+z_i\sin\varphi)/\mathrm{c}]+\omega(f_m,\theta_n,\varphi_k) \quad (1)$$

where $E(f_m,\theta_n,\varphi_k)$ denotes the back-scattering data of radar targets, I denotes the total scattering centers, I denotes the total scattering centers, , x_i, y_i, z_i denote the scattering intensity, scattering type, transversal position parameter, longitudinal position parameter, and vertical position parameter of the i th scattering center respectively. $\mathrm{c}=3\times10^8$ m/s represents the propagation speed of electromagnetic waves and $\omega(f_m,\theta_n,\varphi_k)$ denotes the Gaussian white noise.

$$f_m=f_0+m\Delta f$$

where f_0, Δf, m represent the initial frequency, the frequency step and the frequency index respectively. Similarly,

$$\theta_n=\theta_0+n\Delta\theta,$$

$$\varphi_k=\varphi_0+k\Delta\varphi,$$

where θ_0 and φ_0 are the initial azimuth angle and the initial pitching angle respectively, $n\Delta\theta$ and $k\Delta\varphi$ are the relative small radar rotation angles. The scattering type parameters α_i of typical scattering structures are shown in Table 1 [12].

Table 1 α_i values of typical scattering structures

Typical scattering structure	Value
Flat plate at broad-side, dihedral	1
Singly curved surface reflection	0.5
Point scattering, doubly curved surface	0
Edge diffraction	−0.5
Corner diffraction	−1

As the operating frequency of selected radar satisfies $\Delta f/f_0\ll1$, we can take the following approximation:

$$(f_m/f_0)^{\alpha_i}=(1+m\Delta f/f_0)^{\alpha_i}\approx(1+\alpha_i\Delta f/f_0)^m. \quad (2)$$

Substituting (2) into (1) and transforming the obtained formula to Cartesian coordinates, then using the resampling technique we can get the electromagnetic data of radar targets:

$$E(f_m,\theta_n,\varphi_k)=\sum_{i=1}^{I}B_iP_{xi}^mP_{yi}^nP_{zi}^k+\omega(f_m,\theta_n,\varphi_k),$$
$$m=0,\cdots,M-1;n=0,\cdots,N-1;k=0,\cdots,K-1 \quad (3)$$

where

$$B_i=A_i\exp\left(\mathrm{j}\frac{\pi\alpha_i}{2}-\mathrm{j}\frac{4\pi f_{x0}}{\mathrm{c}}x_i-\mathrm{j}\frac{4\pi f_{y0}}{\mathrm{c}}y_i-\mathrm{j}\frac{4\pi f_{z0}}{\mathrm{c}}z_i\right), \quad (4)$$

$$P_{xi}=\left(1+\alpha_i\frac{\Delta f_x}{f_{x0}}\right)\exp\left(\frac{-4\pi\mathrm{j}\Delta f_xx_i}{\mathrm{c}}\right), \quad (5)$$

$$P_{yi}=\exp\left(\frac{-4\pi\mathrm{j}\Delta f_yy_i}{\mathrm{c}}\right), \quad (6)$$

$$P_{zi}=\exp\left(\frac{-4\pi\mathrm{j}\Delta f_zz_i}{\mathrm{c}}\right), \quad (7)$$

$$\begin{cases}\Delta f_x=\Delta f,\ \ f_{x0}=f_0\\ \Delta f_y=f_0\times\left(\sin\dfrac{\theta_1}{2}-\sin\dfrac{\theta_0}{2}\right)\\ \Delta f_z=f_0\times\left(\sin\dfrac{\varphi_1}{2}-\sin\dfrac{\varphi_0}{2}\right)\end{cases}. \quad (8)$$

Fig.1 represents the 3D frequency domain data range. The cube in Fig. 1 contains the interpolated data points at equal intervals. f_c represents the intermediate frequence between f_0 to f_m.

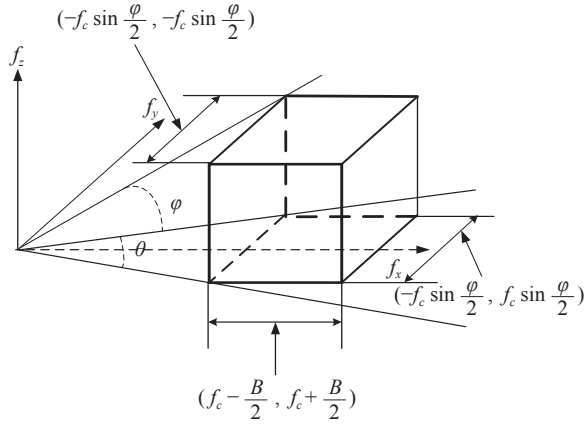

Fig. 1 3D frequency domain data range

Based on (5)−(8), we can estimate x_i, y_i, z_i and α_i by

$$x_i=\frac{-\mathrm{angle}(P_{xi})\times\mathrm{c}}{4\pi\Delta f_x}, \quad (9)$$

$$y_i=\frac{-\mathrm{angle}(P_{yi})\times\mathrm{c}}{4\pi\Delta f_y}, \quad (10)$$

$$z_i = \frac{-\text{angle}(P_{zi}) \times \text{c}}{4\pi \Delta f_z}, \tag{11}$$

$$\alpha_i = (|P_{xi}| - 1) f_0 / \Delta f. \tag{12}$$

3. The proposed algorithm

In this paper, we use the improved 3D-ESPRIT algorithm to estimate the 3D-GTD model parameters. And the extraction processes can be shown as follows.

Step 1 First we perform the spatial smoothing on x direction and a Hankel matrix pencil $\boldsymbol{X}_x$ can be obtained by

$$\boldsymbol{X}_x = \begin{bmatrix} \boldsymbol{X}_0^x & \boldsymbol{X}_1^x & \cdots & \boldsymbol{X}_{M-P}^x \\ \boldsymbol{X}_1^x & \boldsymbol{X}_2^x & \cdots & \boldsymbol{X}_{M-P+1}^x \\ \vdots & \vdots & \ddots & \vdots \\ \boldsymbol{X}_{P-1}^x & \boldsymbol{X}_P^x & \cdots & \boldsymbol{X}_{M-1}^x \end{bmatrix} \tag{13}$$

where

$$\boldsymbol{X}_m^x = \begin{bmatrix} \boldsymbol{x}(m,0) & \boldsymbol{x}(m,1) & \cdots & \boldsymbol{x}(m,K-L) \\ \boldsymbol{x}(m,1) & \boldsymbol{x}(m,2) & \cdots & \boldsymbol{x}(m,K-L+1) \\ \vdots & \vdots & \ddots & \vdots \\ \boldsymbol{x}(m,L-1) & \boldsymbol{x}(m,L) & \cdots & \boldsymbol{x}(m,K-1) \end{bmatrix}, \tag{14}$$

$$\boldsymbol{x}(m,k) = \begin{bmatrix} E(m,0,k) & E(m,1,k) & \cdots & E(m,N-Q,k) \\ E(m,1,k) & E(m,2,k) & \cdots & E(m,N-Q+1,k) \\ \vdots & \vdots & \ddots & \vdots \\ E(m,Q-1,k) & E(m,Q,k) & \cdots & E(m,N-1,k) \end{bmatrix}. \tag{15}$$

Denote three matrix pencil parameters P, Q and L [15], where $P \in [I+1, M-I+1]$, $Q \in [I+1, N-I+1]$, $L \in [I+1, K-I+1]$. M, N, K, I represent the numbers of frequency steps, azimuth angle steps, pitching angle steps and scattering centers respectively.

Step 2 Then a permutation matrix $\boldsymbol{J}$ of size $PQL \times PQL$ is defined as

$$\boldsymbol{J} = \begin{bmatrix} 0 & \cdots & 0 & 1 \\ 0 & \cdots & 1 & 0 \\ \vdots & \iddots & \vdots & \vdots \\ 1 & \cdots & 0 & 0 \end{bmatrix}_{PQL \times PQL}. \tag{16}$$

Based on $\boldsymbol{J}$ and original scattered data $\boldsymbol{X}_x$, a new matrix $\boldsymbol{E}_{conj}$, which possesses the covariance information of the original scattered data $\boldsymbol{X}_x$, can be obtained by

$$\boldsymbol{E}_{conj} = \boldsymbol{J} \cdot \boldsymbol{X}_x. \tag{17}$$

Step 3 Then we can obtain three covariance matrices as follows:

$$\boldsymbol{R}_{X_x X_x} = \boldsymbol{X}_x \boldsymbol{X}_x^{\text{H}}, \tag{18}$$

$$\boldsymbol{R}_{E_{conj} E_{conj}} = \boldsymbol{E}_{conj} \boldsymbol{E}_{conj}^{\text{H}}, \tag{19}$$

$$\boldsymbol{R}_{X_x E_{conj}} = \boldsymbol{X}_x \boldsymbol{E}_{conj}^{\text{H}}, \tag{20}$$

where $(\cdot)^{\text{H}}$ denotes the Hermite transpose.

Step 4 By averaging the three covariance matrices obtained in (18)−(20), a novel total covariance matrix $\boldsymbol{R}$ leads to

$$\boldsymbol{R} = \frac{\boldsymbol{R}_{X_x X_x} + \boldsymbol{R}_{E_{conj} E_{conj}} + \boldsymbol{R}_{X_x E_{conj}}}{3}. \tag{21}$$

Step 5 As $\boldsymbol{R}$ is a Hermitten matrix and thus it satisfies $\boldsymbol{R}$=$\boldsymbol{R}^{\text{H}}$. By squaring the matrix $\boldsymbol{R}$, the final covariance matrix $\boldsymbol{R}_1$ can be obtained as

$$\boldsymbol{R}_1 = \boldsymbol{R}\boldsymbol{R}^{\text{H}} = \boldsymbol{R}^2. \tag{22}$$

Then we have

$$\begin{cases} \lambda_{1i} = \lambda_i^2 \\ \boldsymbol{\Lambda}_{1i} = \boldsymbol{\Lambda}_i \end{cases} \tag{23}$$

where λ_{1i} and $\boldsymbol{\Lambda}_{1i}$ are the eigenvalue and the eigenvector of $\boldsymbol{R}_1$ respectively, λ_i and $\boldsymbol{\Lambda}_i$ are the eigenvalue and the eigenvector of $\boldsymbol{R}$ respectively, $i = 1, 2, \cdots, I$.

From (23), we can observe that the eigenvalues of $\boldsymbol{R}_1$ are equal to two times of $\boldsymbol{R}$. Therefore, by constructing the final covariance matrix $\boldsymbol{R}_1$, the differences between the noise eigenvalues and the signal eigenvalues can be broadened. The variance of estimated parameters is derived as (24) and it is the motivation why we square the total covariance matrix $\boldsymbol{R}$ as well.

$$\text{E}\{(\hat{\xi} - \xi)^2\} = \frac{\dfrac{\sigma^2}{2MNK} \displaystyle\sum_{i=1}^{I} \frac{\gamma_i}{(\sigma^2 - \gamma_i)^2} \left| \boldsymbol{G}^{\text{H}} \cdot \boldsymbol{v}_i^{\text{H}} \right|^2}{\displaystyle\sum_{i=I+1}^{MNK} \left| \frac{\text{d}\boldsymbol{G}^{\text{H}}}{\text{d}z} \cdot \boldsymbol{v}_i^{\text{H}} \right|^2} \tag{24}$$

where $\text{E}\{(\hat{\xi} - \xi)^2\}$ represents the variance of the estimated parameters, $\hat{\xi}$ and ξ represent the estimated parameter and the original parameter respectively, σ^2 and γ_i denote the eigenvalues of noises and eigenvalues of signals respectively, $\boldsymbol{v}_i = \gamma_i \boldsymbol{I} - \boldsymbol{X}^x$ represents the eigenmatrix of γ_i, $\boldsymbol{I}$ represents a $[P \times Q \times L] \times [P \times Q \times L]$ identit matrix, P, Q, L, M, N, and K have been defined in (15).

It can be noticed from (24) that $\text{E}\{(\hat{\xi} - \xi)^2\}$ will be smaller as σ^2 and γ_{m} differs a lot with each other. In this way, more accurate scattering center parameters can be

obtained. Therefore, constructing $\boldsymbol{R}$ can broaden the differences between σ^2 and γ_{m} as well as estimate the GTD model parameters more accurately.

Step 6 Then the singular value decomposition of the novel constructed covariance matrix $\boldsymbol{R}_1$ leads to

$$\boldsymbol{R}_1 = \boldsymbol{U}_{xS}\boldsymbol{D}_{xS}\boldsymbol{V}_{xS}^{\mathrm{H}} + \boldsymbol{U}_{xN}\boldsymbol{D}_{xN}\boldsymbol{V}_{xN}^{\mathrm{H}} \tag{25}$$

where $\boldsymbol{U}_{xS}$, $\boldsymbol{D}_{xS}$ and $\boldsymbol{V}_{xS}$ contain the I principal components, the singular values and the singular vectors related to the signal subspace of x direction. While $\boldsymbol{U}_{xN}$, $\boldsymbol{D}_{xN}$ and $\boldsymbol{V}_{xN}$ contain the remaining components.

Step 7 Construct a matrix $\boldsymbol{F}_x$ as follows:

$$\boldsymbol{F}_x = \underline{\boldsymbol{U}}_{xS}^{+}\overline{\boldsymbol{U}}_{xS} \tag{26}$$

where $(\cdot)^{+}$ denotes the generalized inverse. $\underline{\boldsymbol{U}}_{xS}$ denotes the first $(P-1)QL$ rows of the matrix $\boldsymbol{U}_{xS}$, $\overline{\boldsymbol{U}}_{xS}$ denotes the last $(P-1)QL$ rows of the matrix $\boldsymbol{U}_{xS}$.

Step 8 Based on [15], we can derive the permutation matrices $\boldsymbol{E}_{xy}$ and $\boldsymbol{E}_{yz}$ as

$$\boldsymbol{E}_{xy} = \sum_{q=1}^{Q}\sum_{l=1}^{L}\sum_{p=1}^{P}\boldsymbol{E}_{q,l}^{Q\times L}\otimes\boldsymbol{E}_{l,p}^{L\times P}\otimes\boldsymbol{E}_{p,q}^{P\times Q}, \tag{27}$$

$$\boldsymbol{E}_{yz} = \sum_{l=1}^{L}\sum_{p=1}^{P}\sum_{q=1}^{Q}\boldsymbol{E}_{l,p}^{L\times P}\otimes\boldsymbol{E}_{p,q}^{P\times Q}\otimes\boldsymbol{E}_{q,l}^{Q\times L}, \tag{28}$$

where symbol $\otimes$ denotes Kronecker product, $\boldsymbol{E}_{q,l}^{Q\times L}$ is a matrix of size $Q\times L$ with 1 for (q,l) elements and 0 elsewhere, $\boldsymbol{E}_{l,p}^{L\times P}$ is a matrix of size $L\times P$ with 1 for (l,p) elements and 0 elsewhere, $\boldsymbol{E}_{p,q}^{P}$ is a matrix of size $P\times Q$ with 1 for (p,q) elements and 0 elsewhere. Then according to the relations among x direction, y direction and z direction, we can get the following equations:

$$\boldsymbol{U}_{ys} = \boldsymbol{E}_{xy}\boldsymbol{U}_{xS}, \tag{29}$$

$$\boldsymbol{U}_{zs} = \boldsymbol{E}_{yz}\boldsymbol{U}_{yS}, \tag{30}$$

where $\boldsymbol{U}_{ys}$ contains the I principal components related to the signal subspace of y direction, and $\boldsymbol{U}_{zs}$ contains the I principal components related to the signal subspace of z direction.

Based on obtained matrices $\boldsymbol{U}_{ys}$ and $\boldsymbol{U}_{zs}$, we can calculate $\boldsymbol{F}_y$ and $\boldsymbol{F}_z$ as

$$\boldsymbol{F}_y = \underline{\boldsymbol{U}}_{yS}^{+}\overline{\boldsymbol{U}}_{yS}, \tag{31}$$

$$\boldsymbol{F}_z = \underline{\boldsymbol{U}}_{zS}^{+}\overline{\boldsymbol{U}}_{zS}. \tag{32}$$

Step 9 Calculate the principal eigenvectors of $\boldsymbol{F}_x$, $\boldsymbol{F}_y$ and $\boldsymbol{F}_z$:

$$\begin{cases}\boldsymbol{F}_x + (1-\beta)\boldsymbol{F}_y/2 + (1-\beta)\boldsymbol{F}_z/2 = \boldsymbol{T}^{-1}\boldsymbol{D}\boldsymbol{T}\\ \boldsymbol{\Psi}_x = \boldsymbol{T}\boldsymbol{F}_x\boldsymbol{T}^{-1}\\ \boldsymbol{\Psi}_y = \boldsymbol{T}\boldsymbol{F}_y\boldsymbol{T}^{-1}\\ \boldsymbol{\Psi}_z = \boldsymbol{T}\boldsymbol{F}_z\boldsymbol{T}^{-1}\end{cases} \tag{33}$$

where $(\cdot)^{-1}$ denotes the inverse, and $0<\beta<1$ is a constant. Then the elements, which are on the main diagonal of $\boldsymbol{\Psi}_x$, $\boldsymbol{\Psi}_y$ and $\boldsymbol{\Psi}_z$, consist of P_{xi}, P_{yi} and P_{zi}:

$$\begin{cases}P_{xi} = \mathrm{diag}(\boldsymbol{\Psi}_x)\\ P_{yi} = \mathrm{diag}(\boldsymbol{\Psi}_y)\\ P_{zi} = \mathrm{diag}(\boldsymbol{\Psi}_z)\end{cases} \tag{34}$$

where $i = 1,2,\ldots,I$.

Obviously, the parameters α_i, x_i, y_i, z_i can be estimated by (34) and (9)−(12).

Then the intensity parameter $\tilde{\boldsymbol{A}}$ can be extracted by the least square method as

$$\tilde{\boldsymbol{A}} = (\boldsymbol{G}^{\mathrm{H}}\boldsymbol{G})^{-1}\boldsymbol{G}^{\mathrm{H}}\boldsymbol{E}_{\mathrm{k}} \tag{35}$$

where

$$\boldsymbol{G} = [\boldsymbol{a}_1,\cdots,\boldsymbol{a}_I], \tag{36}$$

$$\begin{aligned}\boldsymbol{a}_i = [&a_i(0,0,0),\cdots,a_i(M-1,0,0),a_i(0,1,0),\cdots,\\ &a_i(M-1,1,0),\cdots,a_i(M-1,N-1,0),\\ &a_i(0,0,1),\cdots,a_i(M-1,N-1,K-1)]^{\mathrm{T}},\end{aligned} \tag{37}$$

$$\begin{aligned}a_i(m,n,k) = \mathrm{j}\left(\frac{f_m}{f_0}\right)^{\alpha_i}\exp\left[\frac{-4\pi\mathrm{j}f_m}{\mathrm{c}}(x_i\cos\theta_n\cos\varphi_k+\right.\\ \left.y_i\sin\theta_n\cos\varphi_k + z_i\sin\varphi_k)\right],\end{aligned} \tag{38}$$

$$\begin{aligned}\boldsymbol{E}_k = [&E(f_0,\theta_0,\varphi_0),\cdots,E(f_{M-1},\theta_0,\varphi_0),a_i(f_0,\theta_1,\varphi_0),\cdots,\\ &a_i(f_{M-1},\theta_1,\varphi_0),\cdots,a_i(f_{M-1},\theta_{N-1},\varphi_0),\\ &a_i(f_0,\theta_0,\varphi_1),\cdots,a_i(f_{M-1},\theta_{N-1},\varphi_{K-1})],\end{aligned} \tag{39}$$

where $(\cdot)^{\mathrm{T}}$ denotes the transpose.

The key idea of our proposed algorithm is from (16)−(24). By constructing the conjugated form of original back-scattering data, we raise the utilization of original data. Then we combine the auto-correlation matrices and the cross-correlation matrix by averaging them. Finally, we square the covariance matrix to broaden the differences between eigenvalues of noise and eigenvalues of signals. Theoretical analysis verifies that our proposed algorithm can improve the accuracy of GTD model parameters. The summary of our proposed algorithm is shown as follows:

Input: back-scattering data $E(f_m,\theta_n,\varphi_k)$

Output: parameters of 3D-GTD model $\{A_i,\alpha_i,x_i,y_i,z_i\}$

Step 1 Construct a Hankel matrix pencil $\boldsymbol{X}_x$.

Step 2 Construct the conjugated matrix of $\boldsymbol{X}_x$, namely $\boldsymbol{E}_{conj}$, and compute covariance matrices $\boldsymbol{R}_{\boldsymbol{X}_x\boldsymbol{X}_x}$, $\boldsymbol{R}_{\boldsymbol{E}_{conj}\boldsymbol{E}_{conj}}$ and $\boldsymbol{R}_{\boldsymbol{X}_x\boldsymbol{E}_{conj}}$.

Step 3 Compute the average matrix.

$$\boldsymbol{R}=\frac{\boldsymbol{R}_{\boldsymbol{X}_x\boldsymbol{X}_x}+\boldsymbol{R}_{\boldsymbol{E}_{conj}\boldsymbol{E}_{conj}}+\boldsymbol{R}_{\boldsymbol{X}_x\boldsymbol{E}_{conj}}}{3}$$

Step 4 Square the matrix $\boldsymbol{R}$ and obtain the final covariance matrix $\boldsymbol{R}_1$.

Step 5 Perform subspace decomposition to get $\boldsymbol{U}_{xS}$, and then construct matrices $\underline{\boldsymbol{U}}_{xS}$ and $\overline{\boldsymbol{U}}_{xS}$.

Step 6 Derive the permutation matrices $\boldsymbol{E}_{xy}$ and $\boldsymbol{E}_{yz}$, and obtain matrices $\boldsymbol{U}_{ys}=\boldsymbol{E}_{xy}\boldsymbol{U}_{xS}$ and $\boldsymbol{U}_{zs}=\boldsymbol{E}_{yz}\boldsymbol{U}_{yS}$.

Step 7 Calculate eigenvalue matrices as $\boldsymbol{F}_y=\underline{\boldsymbol{U}}_{yS}^{+}\overline{\boldsymbol{U}}_{yS}$ and $\boldsymbol{F}_z=\underline{\boldsymbol{U}}_{zS}^{+}\overline{\boldsymbol{U}}_{zS}$, then obtain

$$\boldsymbol{F}_x+(1-\beta)\boldsymbol{F}_y/2+(1-\beta)\boldsymbol{F}_z/2=\boldsymbol{T}^{-1}\boldsymbol{D}\boldsymbol{T},$$

$$\boldsymbol{\Psi}_x=\boldsymbol{T}\boldsymbol{F}_x\boldsymbol{T}^{-1},\boldsymbol{\Psi}_y=\boldsymbol{T}\boldsymbol{F}_y\boldsymbol{T}^{-1},\boldsymbol{\Psi}_z=\boldsymbol{T}\boldsymbol{F}_z\boldsymbol{T}^{-1}.$$

Step 8 Obtain $P_{xi}=\mathrm{diag}(\boldsymbol{\Psi}_x)$, $P_{yi}=\mathrm{diag}(\boldsymbol{\Psi}_y)$, $P_{zi}=\mathrm{diag}(\boldsymbol{\Psi}_z)(i=1,2,\cdots,I)$.

Step 9 Compute parameters of the 3D-GTD model as

$$x_i=\frac{-\mathrm{angle}(P_{xi})\times \mathrm{c}}{4\pi\Delta f_x},$$

$$y_i=\frac{-\mathrm{angle}(P_{yi})\times \mathrm{c}}{4\pi\Delta f_y},$$

$$z_i=\frac{-\mathrm{angle}(P_{zi})\times \mathrm{c}}{4\pi\Delta f_z},$$

$$\alpha_i=\frac{(|P_{xi}|-1)f_0}{\Delta f},$$

and

$$A_i=\mathrm{diag}(\tilde{\boldsymbol{A}})=\mathrm{diag}((\boldsymbol{G}^{\mathrm{H}}\boldsymbol{G})^{-1}\boldsymbol{G}^{\mathrm{H}}\boldsymbol{E}_{\mathrm{k}}).$$

4. Cramer-Rao bound (CRB) analysis

In this section, we derive the closed-form expression of the deterministic CRB of GTD scattering center model parameters. To simplify the derivation, we first consider reducing the 3D-GTD model to the 1D-GTD model. The 1D-GTD model can be expressed as

$$E(f_m)=\sum_{i=1}^{I}A_i\exp\left(\frac{-\mathrm{j}4\pi f_0 r_i}{\mathrm{c}}\right)\left(1+\frac{m\Delta f}{f_0}\right)^{\alpha_i}\cdot \exp\left(\frac{-\mathrm{j}4\pi m\Delta f r_i}{\mathrm{c}}\right)+\omega(f_m)=\sum_{i=1}^{I}a_i\left(1+\frac{m\Delta f}{f_0}\right)^{\alpha_i}\exp(-\mathrm{j}m\varpi_i)+\omega(f_m) \tag{40}$$

where r_i, α_i, A_i represent the position parameter, the scattering intensity and the scattering type of the ith scattering center, respectively. And the other factors are defined as same as (1). Here $a_i=A_i\cdot\exp(-\mathrm{j}4\pi f_0 r_i/\mathrm{c})=a_{\mathrm{Re}i}+\mathrm{j}a_{\mathrm{Im}i}=|a_i|\mathrm{e}^{\mathrm{j}\varphi_i}$ and $\varpi_i=-4\pi\Delta f r_i/\mathrm{c}$.

Hence all parameters in (40) to be estimated can be expressed as follows:

$$\boldsymbol{\zeta}=[\ \sigma^2\quad \boldsymbol{\zeta}_{a\mathrm{Re}}^{\mathrm{T}}\quad \boldsymbol{\zeta}_{a\mathrm{Im}}^{\mathrm{T}}\quad \boldsymbol{\zeta}_{P}^{\mathrm{T}}\quad \boldsymbol{\zeta}_{\varpi}^{\mathrm{T}}\quad]^{\mathrm{T}} \tag{41}$$

where σ^2 denotes the variance of the white noise, $\boldsymbol{\zeta}_{a\mathrm{Re}}^{\mathrm{T}}=[a_{\mathrm{Re}1},\ldots,a_{\mathrm{Re}I}]$, $\boldsymbol{\zeta}_{a\mathrm{Im}}^{\mathrm{T}}=[a_{\mathrm{Im}1},\ldots,a_{\mathrm{Im}I}]$, $\boldsymbol{\zeta}_{P}^{\mathrm{T}}=[p_1,\ldots,p_I]$, $\boldsymbol{\zeta}_{\varpi}^{\mathrm{T}}=[\varpi_1,\ldots,\varpi_I]$.

While the relative operating bandwidth of radar satisfies $\gamma=\dfrac{N\Delta f}{f_0}=\dfrac{B}{f_0}\ll 1$, then the following approximation can be obtained:

$$\left(1+m\frac{\Delta f}{f_0}\right)^{\alpha_i}=\exp\left(\alpha_i\cdot\ln\left(m\frac{\Delta f}{f_0}\right)\right)\approx\exp\left(\alpha_i\cdot m\frac{\Delta f}{f_0}\right). \tag{42}$$

Therefore the 1D-GTD model can be approximated as the damped exponentials (DE) model:

$$E_{\mathrm{DE}}(f_m)=\sum_{i=1}^{I}A_i\exp(m\alpha_i\Delta f/f_0)\exp(-4\pi\mathrm{j}f_m r_i/\mathrm{c})+\omega(f_m)=\sum_{i=1}^{I}A_i\nu_i^m+\omega(f_m) \tag{43}$$

where

$$\nu_i^m=p_i\cdot\exp(-4\pi\mathrm{j}f_m r_i/\mathrm{c}),$$

$$p_i=\exp(m\alpha_i\Delta f/f_0).$$

Zhou has verified that the CRB of the DE model and the GTD scattering center model is substitutable by theoretical derivation and simulation experiments [26]. Therefore, in this section we only derive the CRB of the DE model to replace the estimated limit performance of parameters of the GTD scattering center model.

$\omega(f_m)$ is Gaussian white noise, then the ***CRB*** matrix of the DE model can be written as

$$\boldsymbol{CRB}_{\mathrm{DE}}=\begin{bmatrix}\dfrac{\sigma^4}{N} & \boldsymbol{0}_{1\times 4I}\\ \boldsymbol{0}_{4I\times 1} & \dfrac{\sigma^2}{2}\boldsymbol{F}\end{bmatrix}, \tag{44}$$

$$\boldsymbol{F}=\begin{bmatrix}\mathrm{Re}\{\boldsymbol{E}+\boldsymbol{E}\boldsymbol{B}\boldsymbol{\Delta}_1^{-1}\boldsymbol{B}\boldsymbol{E}\} & -\mathrm{Im}\{\boldsymbol{E}+\boldsymbol{E}\boldsymbol{B}\boldsymbol{\Delta}_1^{-1}\boldsymbol{B}\boldsymbol{E}\} & -\mathrm{Re}\{\boldsymbol{E}\boldsymbol{B}\boldsymbol{A}\boldsymbol{\Delta}^{-1}\boldsymbol{P}\} & \mathrm{Im}\{\boldsymbol{E}\boldsymbol{B}\boldsymbol{A}\boldsymbol{\Delta}^{-1}\}\\ \mathrm{Im}\{\boldsymbol{E}+\boldsymbol{E}\boldsymbol{B}\boldsymbol{\Delta}_1^{-1}\boldsymbol{B}\boldsymbol{E}\} & \mathrm{Re}\{\boldsymbol{E}+\boldsymbol{E}\boldsymbol{B}\boldsymbol{\Delta}_1^{-1}\boldsymbol{B}\boldsymbol{E}\} & -\mathrm{Im}\{\boldsymbol{E}\boldsymbol{B}\boldsymbol{A}\boldsymbol{\Delta}^{-1}\boldsymbol{P}\} & -\mathrm{Re}\{\boldsymbol{E}\boldsymbol{B}\boldsymbol{A}\boldsymbol{\Delta}^{-1}\}\\ -\mathrm{Re}\{\boldsymbol{P}\boldsymbol{\Delta}^{-1}\boldsymbol{A}^{\mathrm{H}}\boldsymbol{B}\boldsymbol{E}\} & \mathrm{Im}\{\boldsymbol{P}\boldsymbol{\Delta}^{-1}\boldsymbol{A}^{\mathrm{H}}\boldsymbol{B}\boldsymbol{E}\} & \mathrm{Re}\{\boldsymbol{P}\boldsymbol{\Delta}^{-1}\boldsymbol{P}\} & -\mathrm{Im}\{\boldsymbol{P}\boldsymbol{\Delta}^{-1}\}\\ -\mathrm{Im}\{\boldsymbol{\Delta}^{-1}\boldsymbol{A}^{\mathrm{H}}\boldsymbol{B}\boldsymbol{E}\} & -\mathrm{Re}\{\boldsymbol{\Delta}^{-1}\boldsymbol{A}^{\mathrm{H}}\boldsymbol{B}\boldsymbol{E}\} & \mathrm{Im}\{\boldsymbol{\Delta}^{-1}\boldsymbol{P}\} & \mathrm{Re}\{\boldsymbol{\Delta}^{-1}\}\end{bmatrix}, \tag{45}$$

where $\boldsymbol{0}$ denotes the zero matrix, $\boldsymbol{\Delta}=\boldsymbol{A}^{\mathrm{H}}\boldsymbol{\Delta}_1\boldsymbol{A}$, $\boldsymbol{A}=\mathrm{diag}(a_1,a_2,\cdots,a_I)$, $\boldsymbol{\Delta}_1=\boldsymbol{B}_2-\boldsymbol{B}\boldsymbol{E}\boldsymbol{B}$, $\boldsymbol{B}_2=\boldsymbol{V}^{\mathrm{H}}\boldsymbol{N}^2\boldsymbol{V}$, $\boldsymbol{B}=$

$\boldsymbol{V}^{\mathrm{H}}\boldsymbol{N}\boldsymbol{V}$, $\boldsymbol{V}=[\boldsymbol{\nu}_1,\boldsymbol{\nu}_2,\cdots,\boldsymbol{\nu}_I]$, $\boldsymbol{\nu}_i=v_i^l\cdot[1,v_i,\cdots,v_i^{N-1}]^{\mathrm{T}}$.

$$l=\begin{cases}-(N-1)/2, & N \text{ is odd}\\ -N/2+1, & N \text{ is even}\end{cases}$$

$$\boldsymbol{N}=\mathrm{diag}\left(-\frac{N-1}{2},\ldots,\frac{N-1}{2}\right)$$

$$\boldsymbol{P}=\mathrm{diag}(p_1,p_2,\cdots,p_I)$$

According to (44) and (45), we can observe that it is complicated to identify the CRB of the DE model parameters. While for most of the wide-band radar, it satisfies with $\Delta f/f_0\ll 1$, which is equivalent to $p_i\approx 1$. Therefore, by simplifying the ***CRB*** matrix in (44), we can obtain the CRB of the DE model parameters as follows:

$$CRB_{a_{\mathrm{Re}i}}=CRB_{a_{\mathrm{Im}i}}\approx\frac{\sigma^2}{2N},\tag{46}$$

$$CRB_{\varpi_i}\approx\frac{6\sigma^2}{|a_i|^2N^3},\tag{47}$$

$$CRB_{p_i}\approx\frac{6\sigma^2p_i^2}{|a_i|^2N^3}.\tag{48}$$

Based on (43), we have the exact relation between the DE model parameters and the GTD model parameters:

$$r_i=-\frac{\mathrm{c}}{4\pi\Delta f}\cdot\varpi_i,\tag{49}$$

$$\alpha_i=\frac{f_0}{\Delta f}\cdot\ln p_i,\tag{50}$$

$$A_i=a_i\cdot\exp(\mathrm{j}4\pi f_0r_i/\mathrm{c}).\tag{51}$$

According to (46)−(51), we obtain

$$\mathrm{var}\{r_i\}\geqslant\left(\frac{\mathrm{c}}{4\pi\Delta f}\right)^2\cdot\frac{6\sigma^2}{|a_i|^2N^3}=\frac{3}{2\pi^2}\cdot\frac{1}{\mathrm{SNR}_i},\tag{52}$$

$$\mathrm{var}\{\alpha_i\}\geqslant\left(\frac{f_0}{\Delta f}\right)^2\cdot\frac{6\sigma^2p_i^2}{|a_i|^2N^3}=\frac{6}{\gamma^2\cdot\mathrm{SNR}_i},\tag{53}$$

$$\mathrm{var}\{|A_i|\}\geqslant\frac{\sigma^2}{2N},\tag{54}$$

where SNR_i denotes the peak SNR of the ith scattering center and it satisfies $\mathrm{SNR}_i\approx\dfrac{N|a_i|^2}{\sigma^2}$.

By extending the 1D-GTD model to the 3D-GTD model, we have

$$\mathrm{var}\{\hat{x}_i\}=\mathrm{var}\{\hat{y}_i\}=\mathrm{var}\{\hat{z}_i\}\geqslant\frac{3}{2\pi^2\mathrm{SNR}_{ii}},\tag{55}$$

$$\mathrm{var}\{\hat{\alpha}_i\}\geqslant\frac{6}{\gamma^2\mathrm{SNR}_{ii}},\tag{56}$$

$$\mathrm{var}\{\hat{A}_i\}\geqslant\frac{1}{2\mathrm{SNR}_{ii}},\tag{57}$$

$$\mathrm{SNR}_{ii}\approx\frac{MNK|A_i|^2}{\sigma^2}\tag{58}$$

where σ^2 represents the variance of the white Gaussian noise.

5. Simulation experiments

To assess the parameter estimation performance of the modified 3D-ESPRIT algorithm, we first compare the root-mean-square-error (RMSE) among the classical 3D-ESPRIT algorithm, the algorithm in [15] and the modified algorithm proposed in this paper. Afterwards, we compare the positioning accuracy of the three algorithms. Finally, we apply the parameters estimated by the three algorithms to the 3D-GTD model, which can extrapolate the RCS in the frequency domain versus SNR. All simulations are performed by Matlab 2017A.

Suppose the radar target consists of four scattering centers and the values of parameters are shown in Table 2. We set the initial frequency f_0 as 10 GHz. The frequency step Δf is 16 MHz, the frequency index M is 11, the initial azimuth angle θ_0 is 90°, the angular step $\Delta\theta$ is 0.01°, the frequency index N is 11, the initial pitching angle φ_0 is 90°, the angular step $\Delta\varphi$ is 0.01°, the frequency index K is 11, and the paring parameter β is 0.5.

Table 2 Parameters of the four scattering centers

Scattering center	x_i/m	y_i/m	α_i	A_i
Scattering center 1	1.212	1.100	1.000	6.000
Scattering center 2	1.453	1.253	0.500	5.000
Scattering center 3	1.634	1.802	0	4.000
Scattering center 4	1.823	2.522	1.000	3.000

We add two dimensional Gaussian white noise to the back-scattering data. The SNR is defined as follows:

$$\mathrm{SNR}=10\lg\frac{\sum_{m=1}^{M}\sum_{n=1}^{N}\sum_{k=1}^{K}|\tilde{s}(m,n,k)|^2}{\sum_{m=1}^{M}\sum_{n=1}^{N}\sum_{k=1}^{K}|\omega(m,n,k)|^2},$$
$$m=0,1,\cdots,M;n=0,1,\cdots,N;k=0,1,\cdots,K\tag{59}$$

where

$$\tilde{s}(m,n,k)=E(f_m,\theta_n,\varphi_k)-\omega(m,n,k).\tag{60}$$

Define the RMSE of the GTD model parameter estima-

tion from D Monte Carlo trials as

$$\mathrm{RMSE}(\varsigma)=\sqrt{\frac{\sum_{i=1}^{D}(\varsigma_i-\varsigma)^2}{D}} \tag{61}$$

where ς_i, ς and D represent the estimated parameters of the ith run of the simulation, the true value, and the total trials of Monte Carlo at each SNR respectively.

5.1 Simulation settings

Example 1 RMSE versus SNR

In the first simulation, we investigate the performance of the modified algorithm with respect to the SNR. Based on the four scattering centers shown in Table 2, the matrix beam parameters P, Q , and L are set as 6, SNR varies from 0 dB to 30 dB with interval 2 dB, and 200 Monte Carlo trials are performed at every fixed SNR. Here we only compare the mean RMSE of the four scattering center parameters. The results are shown in Fig. 2– Fig. 6.

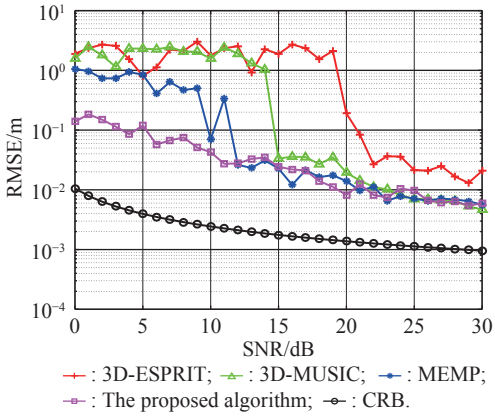

Fig. 2 Mean RMSE of x versus SNR

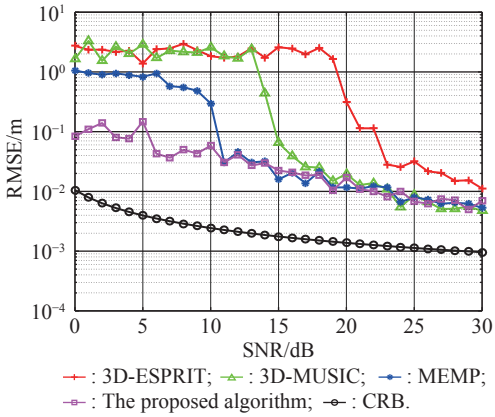

Fig. 3 Mean RMSE of y versus SNR

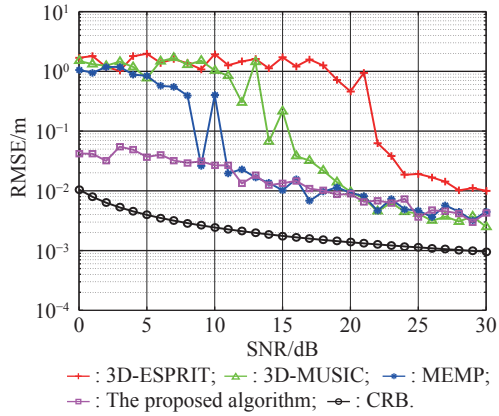

Fig. 4 Mean RMSE of z versus SNR

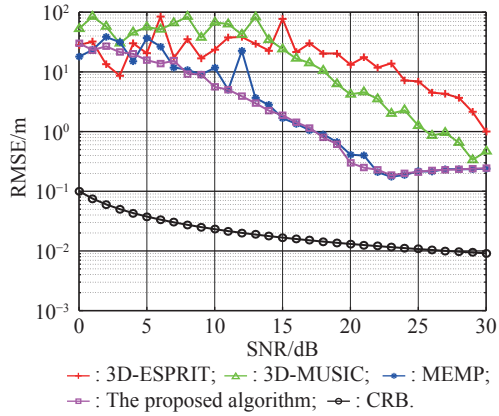

Fig. 5 Mean RMSE of α versus SNR

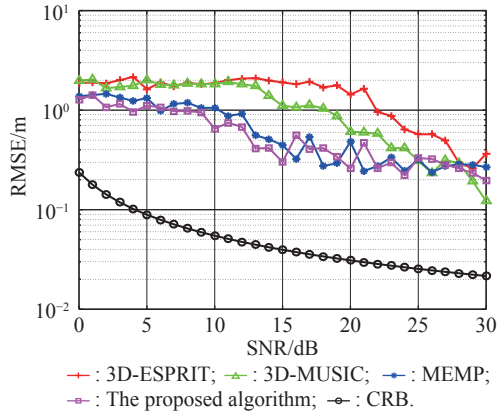

Fig. 6 Mean RMSE of A versus SNR

Example 2 Positioning accuracy analysis

In this example, we verify the positioning accuracy of the proposed algorithm. The simulation conditions are the same as that of Example 1 except that we set SNR as 0 dB and 10 dB. The positioning accuracy of different algorithms at two different values of SNR is shown in Fig.7 and Fig.8.

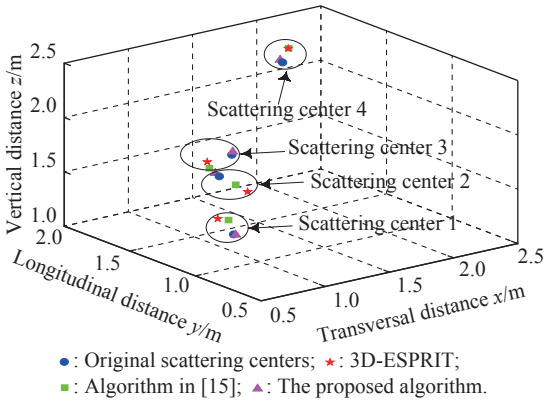

Fig. 7 Positioning accuracy between different algorithms at SNR=0 dB

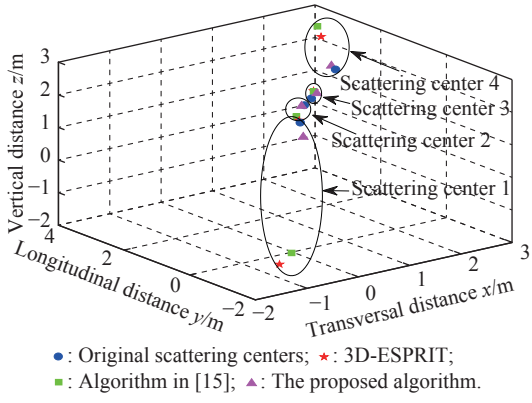

Fig. 8 Positioning accuracy between different algorithms at SNR=10 dB

Example 3 RCS extrapolation accuracy analysis

In this example, we verify the performance of the proposed algorithm by the comparisons of the RCS extrapolation accuracy. The simulation conditions are the same with those of Example 2. Based on the estimated parameters and the relations between electric field and RCS at far fields shown in (62), the RCS of radar targets can be extrapolated in the angular domain. Here we use the back-scattering data of 10 GHz to 10.16 GHz at $\theta=\varphi=90^\circ$ to extrapolate the back-scattering data of 10 GHz to 11.6 GHz at $\theta=\varphi=90^\circ$. The RCS extrapolation accuracy of different algorithms at two different values of SNR is shown in Fig.9 and Fig.10.

$$\sigma(\mathrm{RCS})=\lim_{R\to\infty}4\pi R^2\frac{|\boldsymbol{E}^s|^2}{|\boldsymbol{E}^i|^2} \tag{62}$$

where $\boldsymbol{E}^s$ and $\boldsymbol{E}^i$ represent the scattering electric field and the incident electric field respectively, R represents the far field distance.

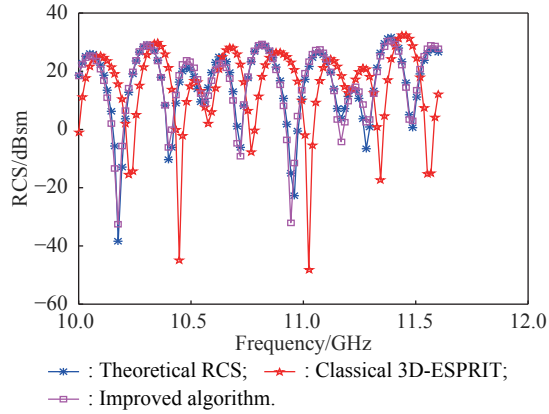

Fig. 9 Comparison between RCS frequency fitting and extrapolation at 90° azimuth and pitching angle (SNR=0 dB)

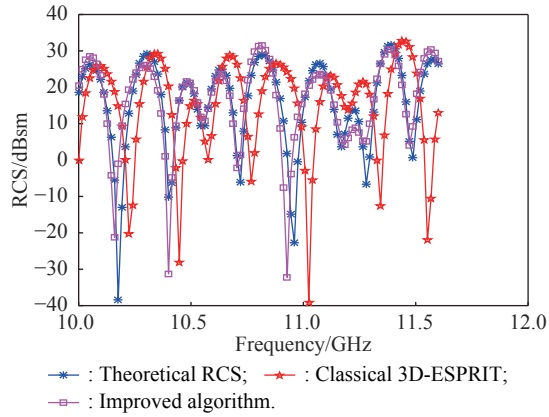

Fig. 10 Comparisons between RCS frequency fitting and extrapolation at 90° azimuth and pitching angle (SNR=10 dB)

Example 4 Computational complexity analysis

The main increase of computational complexity is constructing the novel covariance matrix. Hence we merely compare the computational burden of constructing the covariance matrix, which is shown in Table 3.

Table 3 Comparison of computational burden among different algorithms

Algorithm	Computational burden of constructing covariance matrix
3D-ESPRIT	$P^2Q^2L^2(M-P+1)(N-Q+1)(K-L+1)$
3D-MUSIC	$P^2Q^2L^2(M-P+1)(N-Q+1)(K-L+1)$
Proposed method	$P^2Q^2L^2[3(M-P+1)(N-Q+1)(K-L+1)+2PQL+1]$

5.2 Discussion and analysis

As shown in Fig.2−Fig.6, the RMSE of the GTD model parameters decreases as SNR increases, which verifies the validity of the proposed algorithm. Furthermore, the mean RMSE curve of the proposed algorithm is lower than that of the classical 3D-ESPRIT algorithm, the classical 3D-MUSIC algorithm and the MEMP algorithm,

which indicates the proposed algorithm has a better parameter estimation performance and noise robustness than the other three algorithms for different SNRs.

Additionally, Fig.7 and Fig.8 show that the positioning accuracy of the proposed algorithm is higher than that of the other two algorithms. Similarly, we can observe from Fig.9 and Fig.10 that the reconstructed RCS of the proposed method has a better fitting degree with the theoretical RCS than that of the other two methods. The two simulation results verify the superiority and effectiveness of the proposed algorithm from two different aspects. From Table 3 it is noticed that the proposed algorithm burdens a heavier computational complexity than the other two algorithms.

6. Conclusions

A modified 3D-ESPRIT algorithm with a better parameter estimation performance and more stable noise robustness ability is developed in this paper. The modified algorithm proposes a novel spatial smoothing method and squares the total covariance matrix, which can broaden the differences between eigenvalues of signals and eigenvalues of noises. Simulation results verify the superiority and effectiveness of the proposed algorithm. Furthermore, simulation results indicate that the parameter estimation performance and noise robustness of the modified algorithm are better than that of the classical 3D-ESPRIT algorithm, the classical 3D-MUSIC algorithm and the MEMP algorithm.

References

[1] XU X J. New techniques for radar target scattering signature measurement and processing. Beijing: National Defence Industry Press, 2018: 258−264. (in Chinese)

[2] WU J N, CHEN Y G, FENG D J, et al. Target recognition for polarimetric HRRP based on pre-classification and model matching. Systems Engineering and Electronics, 2016, 38(9): 1969–1974. (in Chinese)

[3] GUO Z H, LI D, ZHANG B Y. Survey of radar target recognition using one-dimensional high range solution profiles. Systems Engineering and Electronics, 2013, 35(1): 53–59. (in Chinese)

[4] ZHUANG Z W, WANG X S, LI X, et al. Radar target recognition. Beijing: Higher Education Press, 2014: 193−200. (in Chinese)

[5] POTTER L C, MOSES R L. Attributed scattering centers for automatic target recognition. IEEE Trans. on Image Processing, 1997, 43(10): 79–91.

[6] DING B Y, WEN G J, HUANG X D, et al. Target recognition in synthetic aperture radar images via matching of attributed scattering centers. IEEE Journal of Selected Topics in Applied Earth Observations and Remote Sensing, 2017, 10(7): 3334–3347.

[7] DING B Y, WEN G J, ZHONG J R, et al. Robust method for the matching of attributed scattering centers with application to synthetic aperture radar automatic target recognition. Journal of Applied Remote Sensing, 2016, 10(1): 016010.

[8] QUAN X Y, ZHANG B C, WANG Z D, et al. An efficient data compression technique based on BPDN for scattered fields from complex targets. Science China: Information Sciences, 2017, 60(10): 109302.

[9] QIU Z Q. Research on radar target scattering center extraction on the spatial estimation algorithm. Chengdu: University of Electronic Science and Technology, 2016. (in Chinese)

[10] WANG J. A study on radar optical region target scattering center extraction and its applications. Nanjing: Nanjing University of Aeronautics and Astronautics, 2010. (in Chinese)

[11] ZHANG Y K, XIAO Y, HU S H. Method of scattering centers association and 3D reconstruction for non-cooperative radar target. Journal of Electronics & Information Technology, 2011, 33(9): 2076–2082. (in Chinese)

[12] POTTER L C, CHANG D M, CARRIER R, et al. A GTD-based parametric model for radar scattering. IEEE Trans. on Antennas and Propagation, 1995, 43(10): 1058–1066.

[13] ZHANG L, HE S Y, ZHU G Q, et al. Forward derivation and analysis for 3-D scattering center position of radar target. Journal of Electronics & Information Technology, 2018, 40(12): 2854–2860. (in Chinese)

[14] ZHONG J R, WEN G J, HUI B W, et al. Three-dimensional positions of attributed scattering centers reconstruction from multiple SAR images based on radar grammetry. Journal of Central South University, 2015, 22(5): 1776–1789. (in Chinese)

[15] STEPHANIE R, MOHAMED N. Estimation of frequencies and damping factors by two-dimensional ESPRIT type methods. IEEE Trans. on Signal Processing, 2001, 49(1): 237–245.

[16] SOULEYMEN S, KONSTANTIN U, PIERRE C. Multidimensional ESPRIT for damped and undamped signals: algorithm, computations, and perturbation analysis. IEEE Trans. on Signal Processing, 2017, 65(22): 5897–5910.

[17] ZHANG W, ZHANG X F, SUN H P, et al. Non-circular generalised-ESPRIT algorithm for direction of arrival estimation. IET Radar, Sonar & Navigation, 2017, 11(5): 736–744.

[18] CHENG Q. A simple modification of ESPRIT. IEEE Signal Processing Letters, 2018, 28(5): 1256–1260.

[19] ZHANG H M, ZHANG H Y. Research on DOA estimation method of sonar radar target based on MUSIC algorithm. Journal of Physics: Conference Series, 2019: 1–5.

[20] CHEN J, GUAN D, TONG Y, et al. Two-dimensional direction of arrival estimation for improved archimedean spiral array with MUSIC algorithm. IEEE Access, 2018, 6: 49740–49745.

[21] ANDREW L K, INDER J G. A modified MUSIC algorithm for direction of arrival estimation in the presence of antenna array manifold mismatch. IEEE Trans. on Antennas and Propagation, 2016, 64(11): 4836–4847.

[22] ZHANG X F, XU L Y, XU L, et al. Direction of departure (DOD) and direction of arrival (DOA) estimation in MIMO radar with reduced dimension MUSIC. IEEE Communication Letters, 2010, 14(12): 1161–1163.

[23] LI H W, ZHANG L, JIANG C Q, et al. Joint TOA and DOA estimation based on improved matrix pencil method. Proc. of the IEEE 4th International Conference on Computer and Communication, 2018: 763−768.

[24] HUANG J Q, GUMPPER K, CHI Y J, et al. Fast two-dimensional super-high resolution image reconstruction algorithm for ultra-high emitter density. Optic-Letters , 2015, 40(13): 2989–2992.

[25] TANG W G, JIANG H, PANG S X, et al. Grid-free DOD and DOA estimation for MIMO radar via duality-based 2D atomic norm minimization. IEEE Access, 2019, 7: 60827–60836.

[26] ZHOU J X. Theory and technology on reconstructing 3D scattering centers of radar targets in optical region. Changsha: National University of Defense Technology, 2006. (in Chinese)

Biographies

ZHENG Shuyu was born in 1996. He received his B.E. degree in fire control and command from Air Force Engineering University, Xi ’an, China, in 2014. Now he is a postgraduate student in Air Force Engineering University. His current research interests include radar signal processing and theory of electromagnetic scattering.
E-mail: 1846372244@qq.com

ZHANG Xiaokuan was born in 1973. He received his B.E. degree in radar engineering from Air Force Engineering University, Xi ’an, China, in 1992, and M.E. and Ph.D. degrees in electronic science and technology from Air Force Engineering University, Xi ’an, China, in 1996 and 2003, respectively. He is currently an professor in the Air and Missile Defense College, Air Force Engineering University, Xi ’an, China. His current research interests include the theory of electromagnetic scattering and radar signal processing, RCS of stealth targets and electronic countermeasure.
E-mail: ezxk@sina.com

ZHAO Weichen was born in 1995. She received her B.E. degree in economics from Changchun Science and Technology, Changchun, China, in 2014. Now she is a postgraduate student in Jilin University of Finance and Economics, Changchun, China. Her current research interests include western economics theory and economics analysis.
E-mail: 2065816439@qq.com

ZHOU Jianxiong was born in 1977. She received her B.E. degree in electronics and M.E. and Ph.D. degrees in information and telecommunication systems from National University of Defense Technology (NUDT), China, in 2000, 2002, and 2006, respectively. She is currently a vice professor in the Automatic Target Recognition Lab, NUDT. Her research interests include target characteristics and radar signal processing.
E-mail: zjxjanet@yahoo.com.cn

ZONG Binfeng was born in 1989. He received his B.E. degree in radar engineering from Air Force Engineering University, Xi ’an, China, in 2010, and M.E. and Ph.D. degrees in electronic science and technology from Air Force Engineering University, Xi ’an, China, in 2012 and 2016, respectively. He is currently an instructor in the Air and Missile Defense College, Air Force Engineering University, Xi ’an, China. His current research interests include aviation electronics, millimeter wave antennas and arrays, and multiple input multiple output radar.
E-mail: zongbinfeng@sina.com

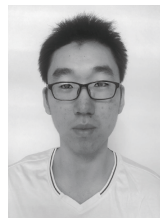

XU Jiahua was born in 1997. He received his B.E. degree in radar engineering from Air Force Engineering University, Xi ’an, China, in 2015. Now he is a postgraduate student in Air Force Engineering University. His current research interests include radar signal processing and theory of electromagnetic scattering.
E-mail: 1019790242@qq.com